Quantification of softening kinetics in cold-rolled pure aluminum and copper using high-temperature scanning indentation

Gabrielle Tiphéne, Guillaume Kermouche, Paul Baral, Claire Maurice, Gaylord Guillonneau, Jean-Michel Bergheau, Warren C. Oliver, Jean-Luc Loubet

Materials & Design 233 (2023) 112171

Contents lists available at ScienceDirect

Materials & Design

journal homepage: www.elsevier.com/locate/matdes

Quantification of softening kinetics in cold-rolled pure aluminum and copper using High-Temperature Scanning Indentation

Gabrielle Tiphéne [a,b,*], Guillaume Kermouche [b], Paul Baral [b], Claire Maurice [b], Gaylord Guillonneau [a], Jean-Michel Bergheau [c], Warren C. Oliver [d], Jean-Luc Loubet [e]

[a] Univ Lyon, Ecole Centrale de Lyon, CNRS, ENTPE, Laboratoire de Tribologie et Dynamique des Systèmes, UMR5513, 69130 Ecully, France
[b] Mines Saint-Etienne, CNRS, UMR5307 LGF, Centre SMS, 42023 Saint Etienne, France
[c] Univ Lyon, Ecole Centrale de Lyon, CNRS, ENTPE, Laboratoire de Tribologie et Dynamique des Systèmes, UMR5513, ENISE, 42023 Saint Etienne, France
[d] KLA Corporation, USA
[e] Univ Lyon, CNRS, Ecole Centrale de Lyon, ENTPE, Laboratoire de Tribologie et Dynamique des Systèmes, UMR5513, 69130 Ecully, France

ARTICLE INFO

Keywords:
Nanoindentation
High-temperature
Mechanical properties
Metals
Restoration kinetics

ABSTRACT

The High-Temperature Scanning Indentation (HTSI) method enables the continuous monitoring of various mechanical properties, including Young's modulus, hardness, and creep properties, during specific thermal cycles. In this study, the HTSI method is applied to cold-rolled samples of commercially pure aluminum and oxygen-free high conductivity (OFHC) copper. The observed variations in hardness during heating are attributed to the underlying restoring mechanisms, namely static recovery and static recrystallization. Inverse analyses are performed using established metallurgical models of restoration. The results highlight the influence of the initial deformation state and heating rate on the kinetics parameters. The findings are further supported by Electron-Back Scattering Diffraction measurements. The study concludes by demonstrating the HTSI method's capability to quantify restoration parameters as a function of temperature through a limited number of well-designed HTSI experiments.

1. Introduction

The characterization of mechanical properties at operating temperatures and appropriate scales is crucial for predicting the lifespan of mechanical systems [1–3]. Failure to control these properties can lead to critical failures. In metallic materials, properties like hardness, strain hardening, and creep are closely linked to their microstructure. Elevated temperatures can induce various metallurgical mechanisms, including restoration, precipitation, and phase transformations, which significantly impact mechanical properties. Restoration mechanisms such as recovery and recrystallization [4] contribute to significant softening in crystalline metals over time. However, accurately predicting the kinetics of these mechanisms for design purposes is challenging due to their dependence on the initial microstructure and chemical composition.

Various methods exist for characterizing these phenomena, such as post-mortem hardness measurements [5–8], Electron Back-Scattering Diffraction (EBSD) [4,9,10], X-ray Diffraction (XRD), and Differential Scanning Calorimetry (DSC) [11,12], among others. These methods typically involve post-mortem characterization, where the sample is annealed at a specific temperature and duration, followed by analysis of microstructure and mechanical properties. The responsible mechanisms for observed changes are identified, and their kinetics can be determined. In recent years, in situ characterization techniques have been developed [13–18]. However, these methods are often time-consuming, requiring hours of testing to obtain limited experimental data points.

Advancements in *in-situ* nanoindentation have expanded its application to high-temperature measurements [19]. The introduction of High-Temperature Scanning Indentation (HTSI) has further improved this technique [20]. HTSI enables continuous monitoring of a material's mechanical properties during a thermal cycle. It has been successfully used to detect superplastic flow and crystallization of ZrCu thin-film metallic glass within the vitreous transition temperature range [21]. These advancements provide valuable insights into the mechanical behavior of materials at elevated temperatures, with promising prospects for further research and applications.

* Corresponding author at: Univ Lyon, Ecole Centrale de Lyon, CNRS, ENTPE, Laboratoire de Tribologie et Dynamique des Systèmes, UMR5513, 69130 Ecully, France.
E-mail address: gabrielle.tiphene@ec-lyon.fr (G. Tiphéne).

https://doi.org/10.1016/j.matdes.2023.112171
Received 11 April 2023; Received in revised form 11 July 2023; Accepted 13 July 2023
Available online 22 July 2023

Table 1
Thermal cycle and indentation parameters applied on the different copper samples during the HTSI tests.

Sample	T_{max}	Heating rate	Annealing time	Maximum load	Depth range in T	Number of indents
Cu-600C-5C/min	600 °C	5 °C/min	60 min	25 mN	750 nm to 2500 nm	880
Cu-600C-5C/min-bis	600 °C	5 °C/min	60 min	25 mN	1250 nm to 2500 nm	600
Cu-400C-1C/min	400 °C	1 °C/min	0 min	25 mN	750 nm to 1700 nm	818
Cu-200C-5C/min	200 °C	5 °C/min	2 min	25 mN	750 nm to 900 nm	428
Cu-250C-5C/min	250 °C	5 °C/min	120 min	25 mN	750 nm to 1300 nm	698

This study aims to demonstrate the application of the HTSI method for quantifying restoration phenomena in metals. By conducting carefully designed HTSI measurements, inverse analyses can characterize the kinetics of static recovery and recrystallization as a function of temperature. The technique is applied to cold-rolled pure aluminum and copper samples, two face-centered cubic metals with different stacking fault energies, resulting in differential favoring of recovery or recrystallization depending on the thermal cycle.

The initial section of this paper provides a brief overview of the physical mechanisms involved in static recovery and recrystallization, focusing on classical analytical models commonly used to describe these restoration processes. This is followed by an introduction to the HTSI method and a description of the materials investigated in this study. Subsequently, the experimental results are presented, and the restoration parameters are quantified using an inverse analysis approach based on the previously discussed analytical models.

The final part of the paper discusses the potential of the HTSI method in accelerating the quantification of restoration kinetics in metals and its implications for alloy design. The study highlights the advantages of HTSI in terms of efficiency and its ability to provide valuable insights into the restoration behavior of materials.

2. Modeling of restoration mechanism

This article focuses on two competing softening mechanisms: static recovery and static recrystallization [4]. These mechanisms are influenced by the level of stored energy in the material, which is typically generated through deformation. Both mechanisms aim to reduce the stored energy and restore the material to a more stable state.

2.1. Static recovery

Static recovery, which has been extensively investigated, primarily involves thermally activated annihilation and rearrangement of dislocations into sub-grain boundaries. According to Taylor's relation [6,22]:

$$\sigma = \sigma_y + M\alpha G b\sqrt{\rho} = \sigma_y + \sigma_i \tag{1}$$

with σ_y the yield stress, σ_i the internal stress, $M = 3$ Taylor factor, $\alpha \approx 0.3$ a constant, G the shear modulus, b the Burger's vector and ρ the dislocation density. The decrease in dislocation density over time leads to the softening effect observed in the recovery process. Various analytical models have been proposed to quantify this phenomenon [5–7,23,24].

Kuhlmann et al. [5,23], propose a simple model based on the relaxation of an internal stress. They assume that deformation leads to a uniform distribution of dislocations within the material structure. The evolution of the internal stress σ_i is governed by the following equations [5,23]:

$$\frac{d\sigma_i}{dt} = -K\exp\left(-\frac{U_0 - \beta\sigma_i}{RT}\right) \tag{2}$$

where K and β are constants, R represents the universal gas constant, T denotes the annealing absolute temperature, and U_0 is the activation energy. The exponential term highlights the thermal activation of static recovery and the influence of dislocation density on its kinetics.

Verdier et al. [6] relate the relaxation of internal stress with the rearrangement and annihilation of dislocations, resulting in the following expression:

$$\frac{d\sigma_i}{dt} = -\frac{64\nu_D}{9M^3\alpha^2}\frac{\sigma_i^2}{E}\exp\left(-\frac{U_0}{RT}\right)\sinh\left(\frac{N_A v_0 \sigma_i}{RT}\right) \tag{3}$$

with ν_D the Debye frequency, E the Young's modulus, U_0 the activation energy at the end of the recovery process, N_A Avogadro constant and v_0 the activation volume.

2.2. Static recrystallization

During static recrystallization, new grains, free of dislocations, nucleate and grow replacing the existing microstructure [4]. This phenomenon leads to a reduction in the average dislocation density at the scale of the Representative Elementary Volume, resulting in softening of the material. The extent of recrystallization is quantified by the recrystallized fraction, and its kinetics during isothermal annealing tests is commonly described by the Kolmogorov, Johnson, Mehl, and Avrami (JMAK) law [25–27]:

$$X = 1 - \exp\left(-b\left(t - t_{inc}\right)^n\right) \tag{4}$$

where b combines information on the nucleation and growth rates, t_{inc} is the incubation time and n is the Avrami exponent.

Like recovery, recrystallization is a thermally activated process, i.e., the recrystallization rate increases with temperature. The time to half-recrystallization can be expressed as [4,28]:

$$\frac{1}{t_{0.5}} = \frac{1}{t_i}\exp\left(-\frac{Q_X}{RT}\right) \tag{5}$$

with t_i a characteristic time and Q_X an activation energy. As nucleation and growth are thermally activated mechanisms, the parameter b is described by:

$$b(T) = b_0\exp\left(-\frac{Q_b}{RT}\right) \tag{6}$$

with b_0 a pre-exponential factor and Q_b an activation energy.

3. Materials and methods

3.1. Samples

Copper samples An initial pure Oxygen Free High-thermal Conductivity (OFHC) copper plate was cold rolled on a laboratory rolling mill, resulting in a final thickness of 3 mm, corresponding to a thickness reduction ratio of 85% For the indentation experiments, pancake-like samples with a diameter ranging from 10 mm to 12 mm were cut from the sheets. Prior to the HTSI experiments, all samples underwent standard metallographic preparation, including SiC papers P460, P600, P1200, followed by diamond polishing down to 0.5μm. The samples were subjected to thermal cycles as presented in Table 1. The naming system for the copper samples follows the convention: material - maximum temperature - heating rate. Sample Cu-600C-5C/min underwent the same thermal cycle twice.

Table 2
Thermal cycle and indentation parameters applied on the different aluminum samples during the HTSI tests.

Sample	r	T_{max}	Heating rate	Annealing time	Maximum load	Depth range in T	Number of indents
Al-pre-annealed	85%	325 °C	3 °C/min	30 min	25 mN	1700 nm to 3000 nm	588
Al-r85-300C-3C/min-30 min	85%	300 °C	3 °C/min	30 min	40 mN	1600 nm to 3200 nm	349
Al-r85-325C-3C/min-1h	85%	325 °C	3 °C/min	60 min	25 mN	1300 nm to 3000 nm	622
Al-r85-325C-1C/min-1h	85%	325 °C	1 °C/min	60 min	25 mN	1300 nm to 2900 nm	1587
Al-r85-325C-3C/min-2h	85%	325 °C	3 °C/min	120 min	25 mN	1300 nm to 3000 nm	473
Al-r60-325C-3C/min-2h	60%	325 °C	3 °C/min	120 min	25 mN	1300 nm to 3000 nm	794
Al-r40-325C-3C/min-2h	40%	325 °C	3 °C/min	120 min	25 mN	1300 nm to 3000 nm	825
Al-r40-300C-3C/min-2min	40%	300 °C	3 °C/min	2 min	25 mN	1300 nm to 2200 nm	615

Aluminum samples A similar process was employed for the aluminum samples. The initial material was a 20 mm thick sheet of commercially pure aluminum (>99.5%). The as-received sheet was divided into three sheets. Two of these sheets underwent machining to reduce their thickness to 5 mm and 7.5 mm, respectively. Subsequently, all three sheets were cold-rolled on a laboratory rolling mill, resulting in a final thickness of 3 mm. This corresponds to reduction ratios of 40%, 60%, and 85%. To perform the indentation experiments, pancake-like samples with diameters ranging from 10 mm to 12 mm were cut from the aluminum sheets. One of the samples with a reduction ratio of 85% was annealed in a furnace at 380 °C for 2 hours to serve as a recrystallized reference sample. Prior to the HTSI experiment, all samples underwent standard metallographic preparation. Table 2 provides an overview of the thermal cycles applied to the aluminum samples. The naming system for the aluminum samples follows the convention: material - reduction ratio - maximum temperature - heating rate - annealing time at maximum temperature.

3.2. Indentation apparatus

Nanoindentation tests were conducted using the InSEM HT nanoindentation device (KLA Corporation) located inside a vacuum chamber with a pressure of 1×10^{-2} Pa. For aluminum specimens, the indentation was performed using a diamond Berkovich tip in the setup integrated into a Scanning Electron Microscope VEGA 3 (Tescan) at the LTDS. Copper specimens, on the other hand, were indented using a sapphire tip on the KLA Corporation device located in Tennessee, USA.

Prior to the experiments, tip calibration was carried out on a fused silica sample at ambient conditions, following the methods described by Loubet et al. [29] and Oliver et al. [30]. The specimen mounting procedure followed the guidelines outlined by Minnert et al. [19]. To ensure proper spacing between indents, a minimum distance of $10h_c$ was maintained, where h_c represents the contact depth [31]. Temperature settings and controls during the experiments were conducted following the same methodology as described in the work by Tiphene et al. [20].

3.3. Microstructure characterization

The initial and final microstructures of the electropolished samples were analyzed using Electron Back-Scattering Diffraction (EBSD) technique. The analysis was conducted on a SUPRA 55 VP ZEISS SEM equipped with an Oxford Instruments NordlysII + AZtec EBSD system. Post-processing of the obtained data was performed using the MTEX MATLAB Toolbox [32].

3.4. High-Temperature Scanning Indentation method

The High-Temperature Scanning Indentation (HTSI) technique, introduced in [20], enables the continuous determination of a material's mechanical properties throughout a thermal cycle. By employing a specific 1-second indentation cycle, variations in Young's modulus, hardness, and creep properties can be calculated over a wide temperature range. In this study, only changes in hardness with respect to time and temperature are considered for the quantification of static recovery and recrystallization kinetics.

During each indentation cycle, hardness is derived from the load-displacement curve using Loubet's contact model, which allows for the estimation of the contact depth h_c [20,29]. This choice was motivated by the expected presence of significant pile-up on cold-rolled aluminum and copper samples. According to this model, the contact depth can be expressed as follows:

$$h_c = 1.2\left(h_{max} - \frac{P_{max}}{S_u} + h_0\right) \tag{7}$$

where h_{max} and P_{max} are the maximal depth and load respectively, S_u is the unloading contact stiffness and h_0 is the tip defect. The contact area is then given by:

$$A_c = \pi(\tan(\theta)h_c)^2 \tag{8}$$

with θ the tip equivalent conical angle (70.32° for a Berkovich tip). Hardness H is computed as:

$$H = \frac{P_{max}}{A_c} \tag{9}$$

Reminder on the HTSI method and examples of load-displacement curves obtained on cold-rolled copper can be found in Figure S1 and Figure S2 in the Supplementary Materials.

4. Results

4.1. Cold-rolled copper

Detection of recrystallization The Cu-600C-5C/min sample (red points) undergoes a thermal cycle presented in Fig. 1. Initially, its hardness at room temperature is approximately 1.3 GPa. As the temperature increases, the hardness decreases linearly until reaching 250 °C. At this temperature, a sudden drop in hardness occurs. After the drop, the hardness continues to decrease with temperature, but at a lower slope compared to the range below 250 °C. During the cooling stage, the hardness gradually increases with a constant slope similar to the final heating stage.

At the end of the thermal cycle, hardness of copper at room temperature is around 0.5 GPa, which is nearly three times lower than the initial hardness. This significant softening indicates the activation of restoration mechanisms, with the sudden drop likely attributed to recrystallization. Recovery-induced softening is typically much slower than recrystallization.

Furthermore, it can be noticed that the hardness standard deviation is different before and after the hardness drop. There is a noticeable difference in the standard deviation of hardness before and after the hardness drop. Prior to the drop, the estimated hardness variations at a given temperature are approximately ±0.1 GPa. After the drop, the variations decrease to around ±0.05 GPa. These changes are expected to be influenced by the microstructure. In the cold-rolled state, the deformation is not uniformly distributed, leading to hardness variations due

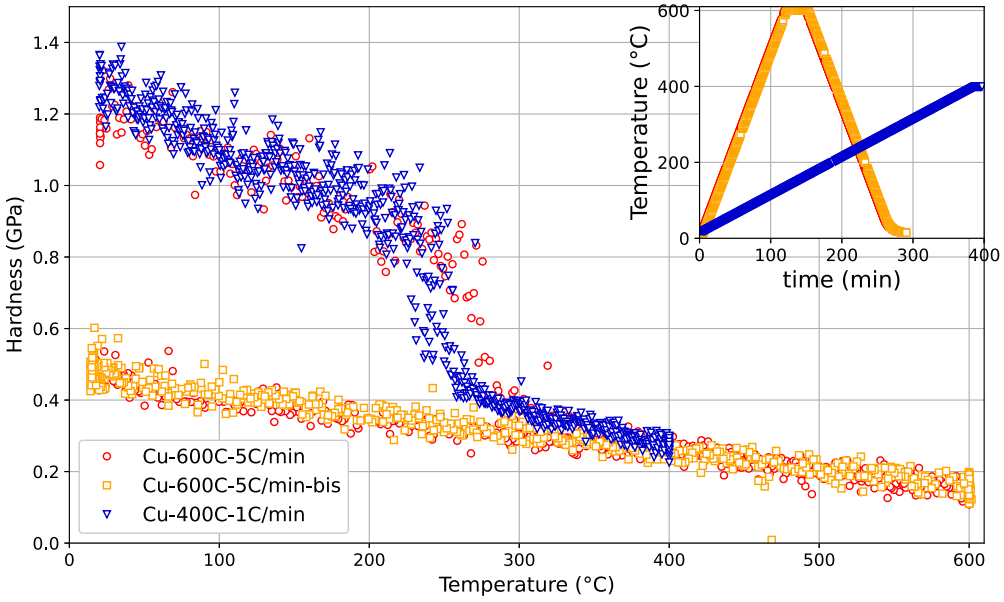

Fig. 1. Effect of heating rates on the hardness changes during an HTSI experiment on pure copper. The drop of hardness during heating is attributed to the recrystallization of the sample. Moreover, decreasing the heating rate decreases the temperature of recrystallization.

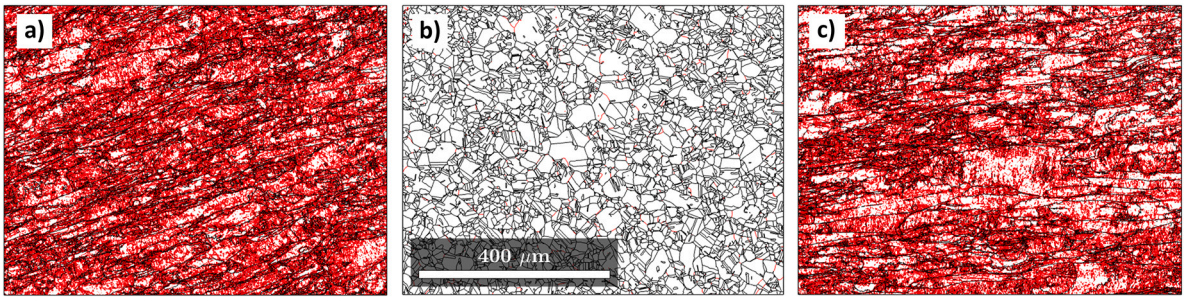

Fig. 2. EBSD measurements were performed on three pure copper samples: (a) the cold-rolled state, (b) sample Cu-600C-5C/min after tests, and (c) sample Cu-200C-5C/min after tests. All three samples are shown in the figures with the same scale. Here, grain boundaries are represented in black, while sub-grain boundaries are shown in red [33,14,34]. From the comparison of the images, it is evident that the recrystallization of sample Cu-600C-5C/min is clearly observed. On the other hand, specimen Cu-200C-5C/min shows a large number of sub-grain boundaries but no clear evidence of recrystallization.

to deformation gradients. In contrast, in the recrystallized sample, the grains are not deformed, and while there may be slight variations in hardness due to grain orientation, the impact appears to be minimal in this case.

When the same thermal cycle is applied once again to the sample Cu-600C-5C/min (sample Cu-600C-5C/min-bis, orange points), it results in a reversible decrease in hardness with temperature, which is consistent with the hardness variations observed during the cooling stage of the first cycle. The hardness standard deviation also remains consistent with that observed during the cooling phase.

This behavior suggests that the sample is likely almost fully recrystallized after the first thermal cycle. This is further confirmed by post-mortem EBSD measurements, as shown in Fig. 2, which indicate a significant recrystallized microstructure. The absence of significant hardness changes during subsequent thermal cycles indicates that the recrystallization process has reached completion, resulting in a stable microstructure.

Impact of heating rate Sample Cu-400C-1C/min (blue points) is submitted to a different thermal cycle: it is heated at 1 °C/min instead of 5 °C/min. Hardness decrease at low temperatures follows the same trend as for sample Cu-600C-5C/min. A sudden drop of hardness is also observed, but it happens at a lower temperature compared to this sample (230 °C instead of 250 °C). Here again the hardness drop is likely the consequence of recrystallization. The standard deviation of hardness also exhibits changes with temperature, consistent with what was observed in sample Cu-600C-5C/min.

Impact of static recovery However, prior to recrystallization, some static recovery may take place in the sample. To verify if this phenomenon occurs, the cold-rolled sample Cu-200C-5C/min is subjected to a different thermal cycle. Since no recrystallization is expected below 200 °C, the sample is heated up to this temperature before being cooled down. As shown in Fig. 3, the hardness changes follow a similar trend as in sample Cu-600C-5C/min at low temperatures. However, in this case, the hardness change with temperature is reversible, indicating the absence of recrystallization or static recovery. Additionally, no changes in the standard deviation of hardness with temperature are observed, which is expected as the structure remains unchanged, and the variations in hardness are primarily influenced by the deformation gradients of the cold-rolled state.

To verify that no recrystallization occurs in sample Cu-200C-5C/min, post-mortem EBSD characterization is performed (see Fig. 2). In contrast to sample Cu-600C-5C/min, no recrystallized grains are detected in sample Cu-200C-5C/min. Therefore, it can be concluded that no recrystallization takes place in this sample. However, to draw definitive conclusions regarding the occurrence of static recovery in copper based on EBSD measurements, more detailed analysis is required. Nevertheless, considering the observed hardness changes in the present testing conditions, it can be inferred that static recovery is not expected

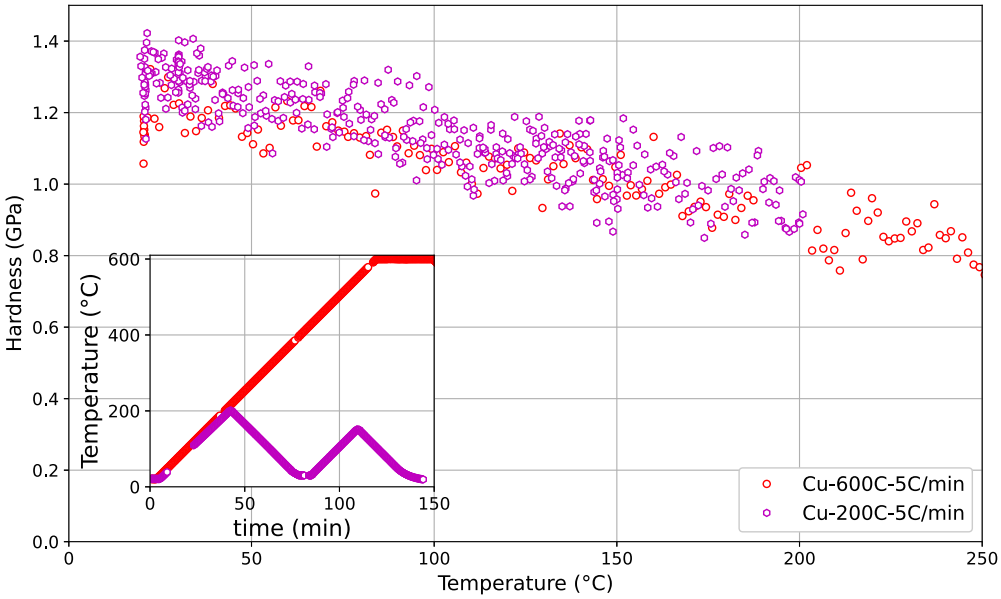

Fig. 3. HTSI experiments on pure copper to detect the static recovery phenomenon. The hardness changes on sample Cu-200C-5C/min are reversible, indicating that no static recovery occurs prior to recrystallization in copper. Note: Due to technical issues, some data points are missing between 50 °C and 100 °C for sample Cu-200C-5C/min.

to occur significantly in copper, and thus it will be neglected in the subsequent analysis.

4.2. Cold-rolled pure aluminum

The same analysis is conducted on aluminum samples, and the results are presented in Fig. 4. Similar to the annealed copper sample Cu-600C-5C/min-bis, the hardness change with temperature of the pre-annealed aluminum sample Al-pre-annealed is reversible. The hardness starts at approximately 0.21 GPa at room temperature and decreases almost linearly with temperature, consistent with the behavior expected for a fully recrystallized sample.

On the other hand, the hardness change of the cold-rolled aluminum sample Al-r85-325C-3C/min-1h is not reversible, similar to what was observed for the cold-rolled Cu-600C-5C/min. However, there are some differences. As the temperature increases, the hardness gradually decreases from approximately 0.4 GPa at room temperature to around 0.07 GPa at the maximum temperature of 325 °C. During this phase, the hardness decreases linearly with temperature, but a slight increase in slope is detected around 250 °C, as previously observed in [20]. During the cooling stage, the hardness increases following the variations observed in the annealed sample. This softening is a clear indication of the activation of restoration mechanisms. However, since there is no sudden drop in hardness, it is difficult to determine whether recrystallization is the only mechanism involved or if recovery also plays a role. Nonetheless, the change in slope is likely a direct consequence of the onset of recrystallization. Regarding the hardness standard variations, it appears that the thermal cycle may have a slight effect on them in the case of sample Al-r85-325C-3C/min-1h.

Impact of heating rate Sample Al-r85-325C-1C/min-1h was heated at a rate of 1 °C/min instead of 3 °C/min. When examining the changes in hardness with temperature, it appears to behave similarly to sample Al-r85-325C-3C/min-1h (see Fig. 4). However, upon closer inspection of the high-temperature zone, a slight variation can be observed. Unlike sample Al-r85-325C-3C/min-1h, there is no change in slope in sample Al-r85-325C-1C/min-1h around 250 °C. The significant decrease in hardness actually occurs during the holding period at high temperature. Interestingly, reducing the heating rate leads to an increase in the temperature at which static recrystallization takes place. This stands in contrast to the observations in copper samples and may indicate a competition between recrystallization and recovery mechanisms, with recovery slowing down recrystallization by reducing the stored energy in the grains (dislocation density).

Moreover, a clear effect of the thermal cycle on the standard deviation of hardness is observed in this sample. Initially, at room temperature (RT), it is estimated to be near ±0.05 GPa, while after the cycle, it reduces to approximately ±0.02 GPa. Interestingly, there is an initial reduction in the standard deviation towards the end of the heating phase. The presence of static recovery leads to a decrease of the deformation gradients: it may explain this first changes in hardness standard deviation.

Impact of initial deformation state Samples Al-r85-325C-3C/min-2h, Al-r60-325C-3C/min-2h, and Al-r40-325C-3C/min-2h were subjected to cold rolling with different thickness reduction ratios. As shown in Fig. 5, their hardness at room temperature (RT) is similar, indicating that the plastic strain level is sufficiently high, resulting in almost no difference in their yield stress. In other words, the strain hardening is nearly maximum. However, when these samples are subjected to the same thermal cycle, slight disparities are observed during the high-temperature regime. The hardness behavior of the three samples is identical up to 250 °C. Beyond this temperature, as shown in the inset of Fig. 5, distinct changes in hardness at high temperature are observed. The softening kinetics is faster for the sample with the highest rolling ratio, i.e., Al-r85-325C-3C/min-2h, and slower for the sample with the lowest rolling ratio, i.e., Al-r40-325C-3C/min-2h. This indicates that the initial deformation state influences the restoration mechanisms involved. At the end of the holding period at 325 °C, the hardness of all specimens converges to the same value, corresponding to the hardness of a fully recrystallized sample.

Impact of static recovery To investigate the occurrence of static recovery in the aluminum sample, sample Al-r40-300C-3C/min-2min, which underwent a thermal cycle up to 300 °C and subsequent cooling, is compared with sample Al-r40-325C-3C/min-2h, as both samples have the same thickness reduction ratio (as indicated in Table 1).

Up to 300 °C, the hardness changes of the two samples are consistent. However, during the cooling phase, sample Al-r40-300C-3C/min-2min shows an increase in hardness but does not fully recover its initial value.

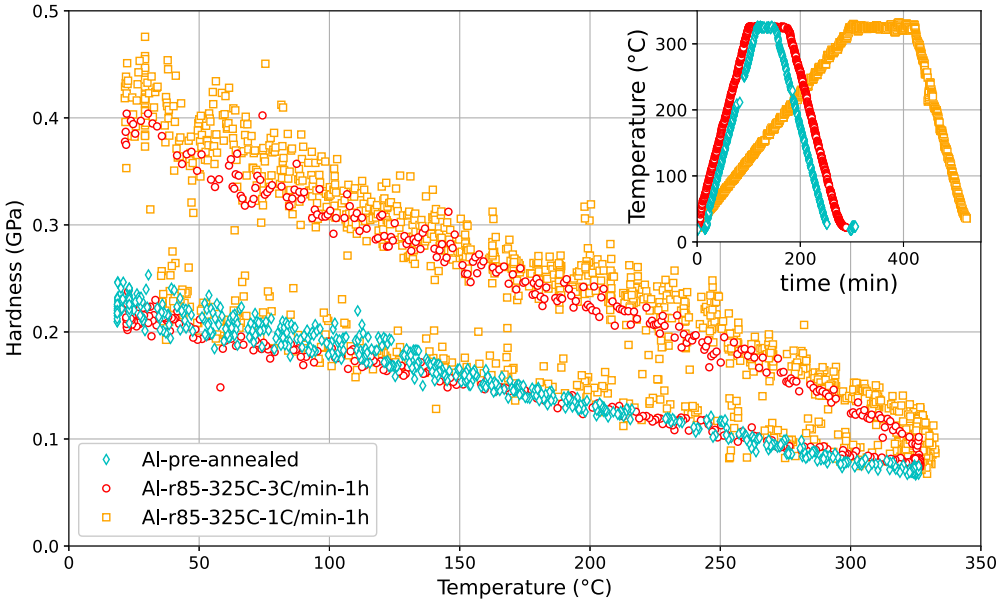

Fig. 4. Effect of heating rates on the hardness changes during an HTSI experiment on pure aluminum (Al-pre-annealed and Al-r85-325C-3C/min-1h: 3 °C/min, Al-r85-325C-1C/min-1h: 1 °C/min). The change in slope of hardness with temperature observed in sample Al-r85-325C-3C/min-1h is indicative of recrystallization. In contrast, for sample Al-r85-325C-1C/min-1h, recrystallization occurs at a higher temperature, suggesting the occurrence of static recovery in aluminum samples, unlike in copper. Note: Due to technical issues, some data points are missing between 210 °C and 230 °C for sample Al-pre-annealed.

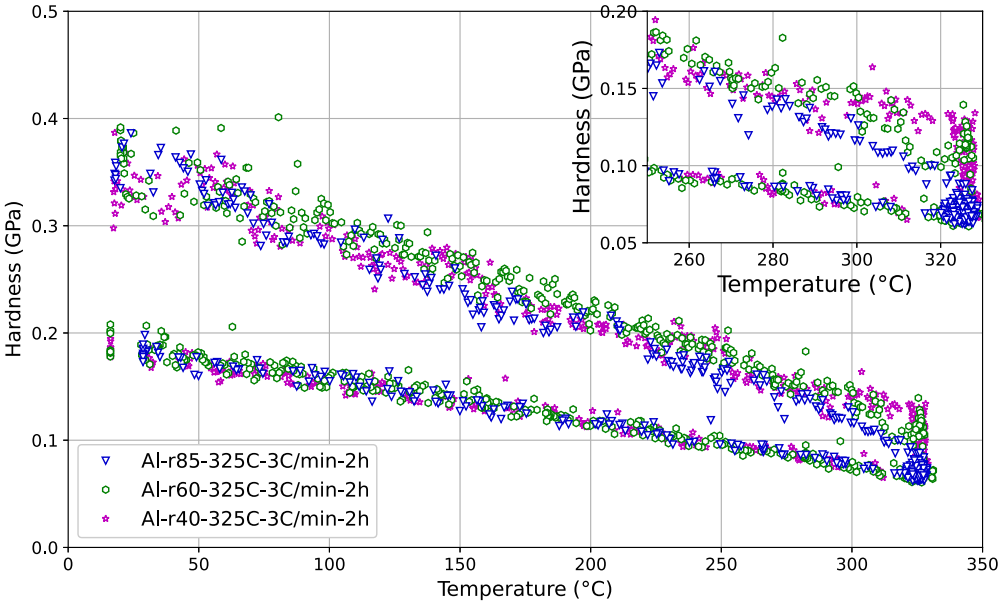

Fig. 5. Effect of the initial deformation state (Al-r85-325C-3C/min-2h: $r = 0.85$, Al-r60-325C-3C/min-2h: $r = 0.60$, Al-r40-325C-3C/min-2h: $r = 0.40$) on the changes of hardness in temperature on pure copper. The samples are heating at 3 °C/min up to 325 °C, maintained during 2 hour before being cooled down at 3 °C/min. The differences at high temperature indicate that the initial cold-rolled state impacts the restoration kinetics.

This indicates that the hardness variations observed in this sample are irreversible. Since the cooling stage starts at a temperature below the onset of recrystallization for this particular rolling ratio, the underlying softening mechanism is likely attributed to static recovery.

Post-mortem electron backscatter diffraction (EBSD) measurements were conducted on the samples, specifically on sample Al-r40-325C-3C/min-2h and Al-r40-300C-3C/min-2min, to further analyze their microstructural characteristics (see Fig. 7). The EBSD results reveal that sample Al-r40-325C-3C/min-2h exhibits a low number of large grains, indicating complete recrystallization of the material. In contrast, sample Al-r40-300C-3C/min-2min displays elongated grains embedded within a dense sub-grain network, which is characteristic of a cold-rolled deformation. However, small recrystallized nuclei (indicated by blue arrows) are also observed in this sample. It is important to note that these nuclei are significantly smaller in size compared to the indentation size used for hardness measurements, suggesting that they are not responsible for the observed hardness decrease during the thermal cycle. Based on these findings, it can be concluded that the observed softening in sample Al-r40-300C-3C/min-2min is likely attributed to the phenomenon of static recovery.

5. Modeling of restoration kinetics

The decrease in hardness with increasing temperature can be attributed to three main mechanisms: thermal activation of plastic flow, static recovery, and recrystallization of the microstructure [4]. To quan-

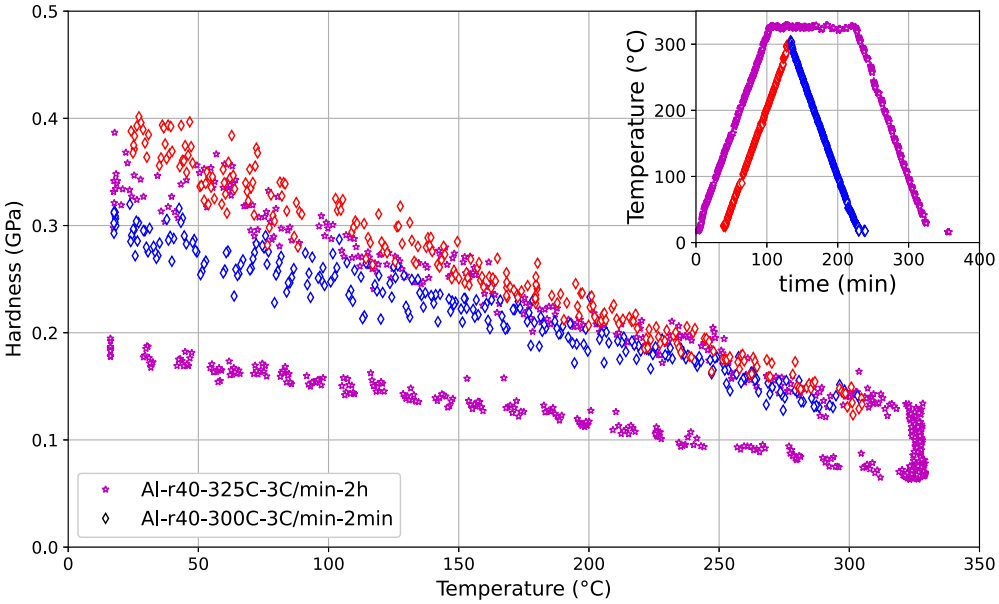

Fig. 6. Detection of static recovery on pure aluminum sample. Sample Al-r40-300C-3C/min-2min is heated up to 300 °C to prevent static recrystallization and verify if static recovery is taking place. The observation of irreversible hardness variations in sample Al-r40-300C-3C/min-2min serves as a clear indication that static recovery is indeed taking place.

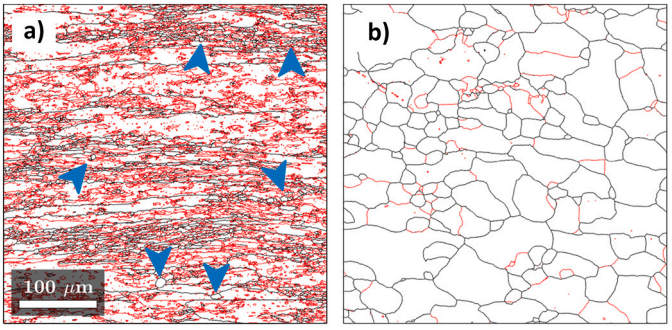

Fig. 7. Post-mortem EBSD measurements on samples with a reduction ratio of 40% (left) after recovery only (sample Al-r40-300C-3C/min-2min), (right) fully recrystallized state (sample Al-r40-325C-3C/min-2h). The grains boundaries are in black and the sub-grains one in red. Nuclei are indicated by arrows. Sample Al-r40-325C-3C/min-2h is in a fully recrystallized state, as indicated by the absence of residual deformed grains. In contrast, sample Al-r40-300C-3C/min-2min shows elongated grains surrounded by a dense sub-grain network. Given the small size of the few detected nuclei, it can be inferred that they are not responsible for the observed softening during the thermal cycle. This softening is likely a consequence of static recovery.

tify the kinetics of each phenomenon, it is necessary to assess their respective contributions to the hardness changes observed during temperature variations. To achieve this, hardness can be transformed into a representative stress value, denoted as σ_r, using the analytical approach developed by Kermouche et al. [35]:

$$\sigma_r = \left(\frac{\xi_3 \cot(\theta)}{\xi_1 \cot(\theta) - (1-\xi_2)\frac{H}{E}} \right) H \tag{10}$$

with the geometrical constants for a Berkovich indenter, $\xi_1 = 0.66$, $\xi_2 = 0.216$ and $\xi_3 = 0.24$.

To separate the impacts of recrystallization, static recovery, and thermal activation of plasticity on the hardness changes, a mixture law is used [36]:

$$\sigma_r(t,T) = X(t,T)\sigma_{ReX}(t,T) + (1 - X(t,T))\sigma_\rho(t,T) \tag{11}$$

with X the recrystallized fraction. σ_{ReX} is the stress of the fully recrystallized state in temperature and varies solely due to the thermal activation of plastic flow. On the other hand, the stress σ_ρ describes the microstructure in the deformed state, which evolves due to the combined effects of thermal activation of plastic flow and static recovery occurring during temperature variations. Details about the modeling steps can be found in the Supplementary Materials.

6. Quantification of restoration kinetics

6.1. Application on cold-rolled copper

As static recovery is not detected in the Cu-200C-5C/min sample, its impact on hardness variations with temperature is considered negligible under the tested conditions. For copper, only thermal activation of plastic flow and static recrystallization will be taken into account.

6.1.1. Quantifying the thermal activation of plastic flow

The thermal activation of plastic flow is characterized by the parameters a_0 and a_{ReX}, which are determined on sample Cu-600C-5C/min. They are obtained by analyzing the heating data between RT and 200 °C or during cooling, respectively. These parameters are assumed to remain constant with temperature, implying that the activation volume also remains constant. This assumption contradicts most models that deal with the thermal activation theory of crystal plasticity [37]. It can be interpreted that the activation volume remains approximately constant over the temperature range studied. This interpretation is coherent in this case since no static recovery is expected to occur.

6.1.2. Quantifying the kinetics of static recrystallization

Once the thermal activation of plastic flow has been characterized, the recrystallized fraction can be computed using equation S19. Subsequently, a Particle Swarm Optimization (PSO) algorithm [38–41] is employed to determine the recrystallization parameters. This algorithm was chosen due to the large number of local minima in the solution space. However, it significantly increases the time required to obtain the results. More details on the application of PSO algorithms in the presented study can be found in the Supplementary Materials. To ensure the uniqueness and stability of the solution, the identifiability factor I, proposed in [42,43], is computed.

Table 3
Recrystallization parameters of copper obtained by Particle Swarm Optimization (PSO).

Sample	Heating rate (°C/min)	t_0 (min)	b_0 (min^{-1})	Q_b (kJ/mol)	n	n_2	I
Cu-600C-5C/min	5	50	3.5×10^9	106	3.58	0.34	4.42
Cu-400C-1C/min	1	50	2.8×10^9	104	3.32	0.34	4.36

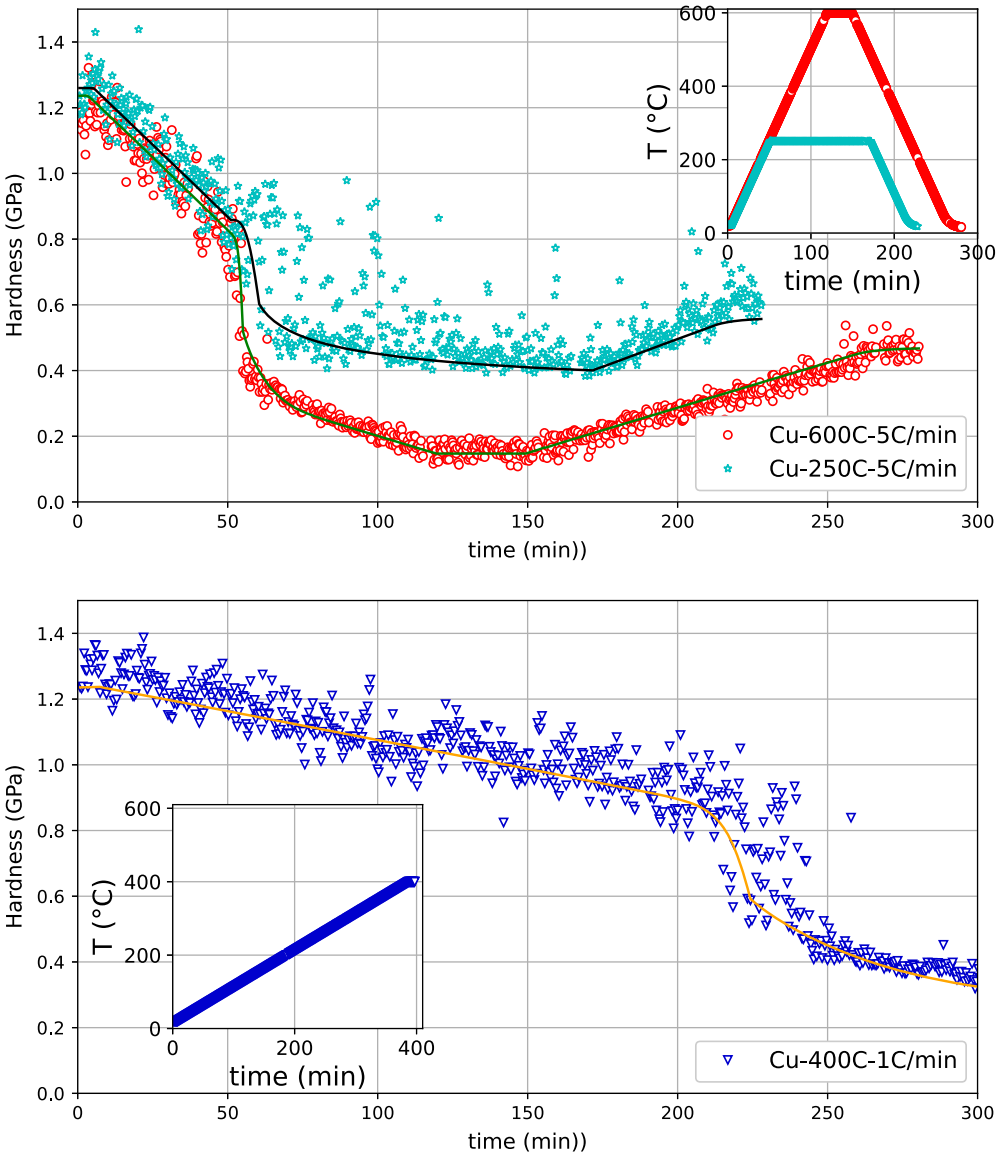

Fig. 8. Hardness changes versus time on pure copper. The recrystallization parameters were determined from sample Cu-600C-5C/min. These parameters enable us to estimate the hardness modifications and corresponding microstructure changes when different thermal cycles are applied, such as for samples Cu-400C-1C/min and Cu-250C-5C/min. The predicted hardness curves for these cases exhibit a remarkable fit to the experimental data.

This inverse methodology is carried out independently on samples Cu-600C-5C/min and Cu-400C-1C/min. The resulting recrystallization parameters from the PSO optimization are presented in Table 3. Fig. 8 displays the hardness versus time curves, demonstrating a remarkable agreement between the experimental data and the JMAK model. Notably, a suitable reconstruction of the onset of recrystallization is achieved, although some discrepancies are observed when the recrystallized fraction exceeds 80%. According to the literature [44,45], the Avrami exponent decreases with increasing recrystallized fraction in copper. To account for this effect, the JMAK formulation was modified accordingly: if the recrystallized fraction is below 0.5, a constant value of n is utilized, whereas if it is above 0.5, a constant value of n_2 is employed.

One interesting observation is that the activation energy for nucleation-growth rates, denoted as Q_b, is similar for both tested conditions. The main difference lies in the parameter b_0, which is slightly lower for the slower heating rate. This difference is likely a consequence of the optimization process. However, it should be noted that b_0 does not significantly depend on the heating rate since recrystallization is the only mechanism occurring in this case [4]. Nevertheless, these results should be interpreted with caution. Firstly, it was not possible to determine a set of parameters that includes incubation, nucleation, and growth rates. For simplicity, the activation energy of incubation, de-

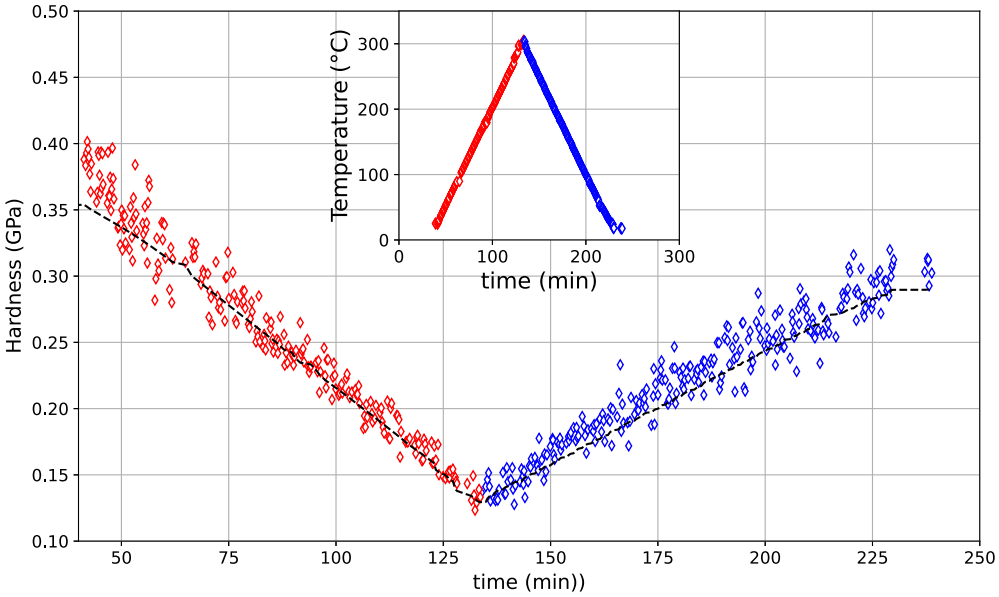

Fig. 9. Hardness modeling of sample Al-r40-300C-3C/min-2min. The static recovery parameters have been identified on sample Al-r40-325C-3C/min-2h.

noted as Q_t, was fixed at 1.0 J/mol. This assumption implies that the incubation time does not depend on temperature, which is highly unlikely. According to Pantleon et al. [28], Q_t and Q_b are expected to be of the same order of magnitude since the underlying mechanisms are all based on atomic jumps. Secondly, the identifiability factor I is greater than 2, indicating that the available data is not sufficiently informative to identify a unique and stable solution. While uniqueness is not achieved, the determined parameter values are very close to each other.

The parameters determined from sample Cu-600C-5C/min are utilized to predict the hardness changes in samples Cu-400C-1C/min and Cu-250C-5C/min. The resulting predictions, shown in Fig. 8, are in good agreement with the experimental data, indicating the reliability of the model. This demonstrates the potential of the inverse methodology in quantifying the kinetics of static recrystallization in copper. Once the parameters are determined, the model can be applied to predict microstructure changes for various thermal cycles. It is evident that the proposed methodology shows promise, although further refinements may still be necessary to improve its accuracy and reliability. As shown in Table 3, the heating rate does not have a significant impact on the kinetics parameters, since recrystallization is the only restoration phenomenon occurring in this case. The observation that recrystallization occurs at a lower temperature with a slower heating rate may seem surprising. However, when heating at a rate of 1 °C/min, recrystallization is detected around 220 min, while it occurs around 50 min when heating at a rate of 5 °C/min. This difference in time is attributed to the fact that when heating slowly, the sample spends more time at each temperature, allowing for the formation of stable nuclei. Consequently, a stable nucleus can be expected to form at a lower temperature when the heating rate is slower. However, it should be noted that this is possible because no other restoration mechanisms that reduce the stored energy of the sample are occurring simultaneously.

6.2. Application on cold-rolled aluminum

6.2.1. Quantifying the thermal activation of plastic flow

The main difference in the case of aluminum is the detection of static recovery, which was evidenced using the Al-r40-300C-3C/min-2min sample (see Fig. 6). This sample is utilized to determine the parameter a_0 through linear fitting of the hardness variations during cooling. Since the hardness decreases linearly with temperature during cooling, it is assumed that a_0 does not vary with temperature. Furthermore, since the temperature dependence of hardness prior to recrystallization is not influenced by the thickness reduction ratio, the same value of a_0 is employed for all samples.

Table 4
Static recovery parameters of cold-rolled aluminum obtained by PSO.

Sample	r	U_0 (kJ/mol)	v_0 (b^3)	$v_0\sigma_0$ (eV)	I
Al-r85-325C-3C/min-2h	85%	207	133	2.68	1.19
Al-r60-325C-3C/min-2h	60%	207	148	2.93	1.70
Al-r40-325C-3C/min-2h	40%	207	153	2.78	1.61

Samples Al-r85-325C-3C/min-2h, Al-r60-325C-3C/min-2h, and Al-r40-325C-3C/min-2h are observed to be fully recrystallized at the end of the thermal cycle. During the heating stage and at the beginning of annealing at 325 °C, recrystallization and static recovery are expected to occur, but they should not take place during the cooling phase. Therefore, the parameter a_{ReX} is evaluated based on the cooling behavior of these samples.

Since room temperature corresponds to approximately one-third of the melting temperature of aluminum, it is reasonable to assume that the activation volume varies only slightly within the studied temperature range. Therefore, it is consistent to consider that the values of a_0 and a_{ReX} remain constant throughout the temperature range of interest.

6.2.2. Quantifying the kinetics of static recovery

A Particle Swarm Optimization (PSO) algorithm [38–41] is then applied to quantify the activation energy and volume of the static recovery process, which are expected to depend on the initial thickness reduction ratio. Table 4 presents the parameters for static recovery based on Verdier's model. Previous studies [6,36,46] have shown that the activation energy remains constant for different cold-rolled states, while the activation volume decreases with increased deformation. The determined activation energy is consistent with literature data [6,36,46]. However, the activation volume appears relatively large compared to data obtained for other aluminum grades. This discrepancy could be attributed to the specific aluminum grade used in this study. Grades containing magnesium tend to have a higher density of defects, resulting in a shorter average free path and thus a reduced activation volume.

The identification factor $I < 2$ indicates a good identifiability of the solution. The reconstructed hardness variations for sample Al-r40-

Table 5
Recrystallization parameters of cold-rolled aluminum samples obtained by PSO optimization.

Sample	r	Heating rate (°C/min)	t_0 (min)	b_0 (min^{-1})	Q_b (kJ/mol)	n	I
Al-r40-325C-3C/min-2h	40%	3	122	10^{10}	127	1	4.95
Al-r60-325C-3C/min-2h	60%	3	100	10^{10}	127	1	4.81
Al-r85-325C-3C/min-2h	85%	3	80	10^{10}	127	1	4.19
Al-r85-325C-1C/min-1h	85%	1	72	8.64×10^9	139	1.22	18.3

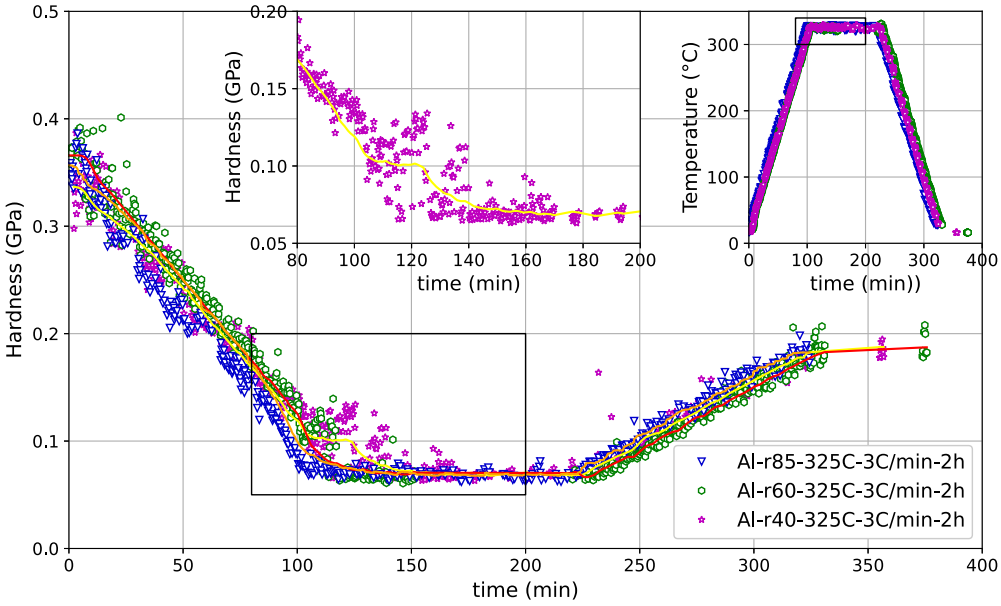

Fig. 10. Modeling of hardness changes of sample Al-r85-325C-3C/min-2h (orange), Al-r60-325C-3C/min-2h (red) and Al-r40-325C-3C/min-2h (yellow). Static recovery and static recrystallization are evaluated by PSO algorithms. The obtained kinetics' parameters allow consistent predictions compared to experimental results. In the zoom on sample Al-r40-325C-3C/min-2h, some scattering in hardness values is obtained when the annealing starts (at 100 min). It is the sign of an heterogeneous recrystallization detected here. The modeling gives a mean evolution of this phenomenon. The kink presents on the yellow curve is related to the issue of modeling the incubation phase here.

300C-3C/min-2min are shown in Fig. 9, demonstrating a convincing agreement between the reconstruction and the experimental data.

6.2.3. Quantifying the kinetics of static recrystallization

Using the identified parameters for thermal activation of plastic flow and static recovery, the recrystallized fraction can now be computed. The Particle Swarm Optimization (PSO) algorithm [38–41] is once again employed to determine the recrystallization parameters, as shown in Table 5. Since the kinetics of recrystallization is expected to be influenced by the initial deformed state and the heating rate, the parameters are determined for samples Al-r85-325C-3C/min-2h, Al-r60-325C-3C/min-2h, Al-r40-325C-3C/min-2h, and Al-r85-325C-1C/min-1h.

Incubation phase The incubation phase is influenced by the recovery process, and therefore, it is expected that the incubation time (t_0) would depend on the heating rate. Let's consider that the sample is initially heated at a certain heating rate (β_{eg}) until a specific recrystallization temperature (T_{eg}) is reached. Now, if the experiment is conducted at a lower heating rate ($\beta < \beta_{eg}$), more time elapses before reaching T_{eg}, allowing for greater recovery of the sample and reducing the amount of stored energy. Consequently, it becomes more challenging to form stable nuclei in the structure, leading to a higher incubation time. Although the activation energy of the incubation phase is assumed to be 1 J/mol, indicating that this phase is not thermally activated, the observed values may not exhibit the expected trend due to the need for a more refined model that accounts for the impact of static recovery on recrystallization kinetics.

A similar analysis can be conducted to examine the impact of the initial deformed state on the incubation time. Since the reduction ratio varies between samples, the stored energy also differs. Consequently, when subjected to the same thermal cycle, the formation of stable nuclei becomes more challenging for samples with a lower thickness reduction ratio, leading to an increase in the incubation time. The observed dependence of t_0 on the thickness reduction ratio aligns with this expectation. However, conducting additional experiments would be beneficial to quantify its dependence more accurately.

Nucleation and growth phase When using a heating rate of 3 °C/min, it appears that the initial deformed state does not have a significant impact on the growth parameters. The optimization algorithm yields the same prefactor b_0, activation energy of nucleation and growth Q_b, and Avrami coefficient n for all samples. The obtained activation energy of growth is comparable to the activation energy of self-diffusion in aluminum [47]. This finding aligns with the conclusions drawn by Pantleon et al. [28], providing further consistency to the results.

The observed effect of the heating rate on the results is in line with the presence of static recovery, which reduces the stored energy and consequently can delay the onset of recrystallization. The parameters related to nucleation and growth in sample Al-r85-325C-1C/min-1h differ from those of sample Al-r85-325C-3C/min-2h but still exhibit similar magnitudes. This dependency of recrystallization kinetics on both heating rate and initial deformation state is consistent with expectations.

Similar to copper, it is not possible to obtain a unique and stable solution for the parameters of recrystallization kinetics in aluminum. The identification factor remains higher than 2, indicating that the available data are not sufficient to achieve a robust and reliable solution. However, despite this limitation, the parameters obtained for static re-

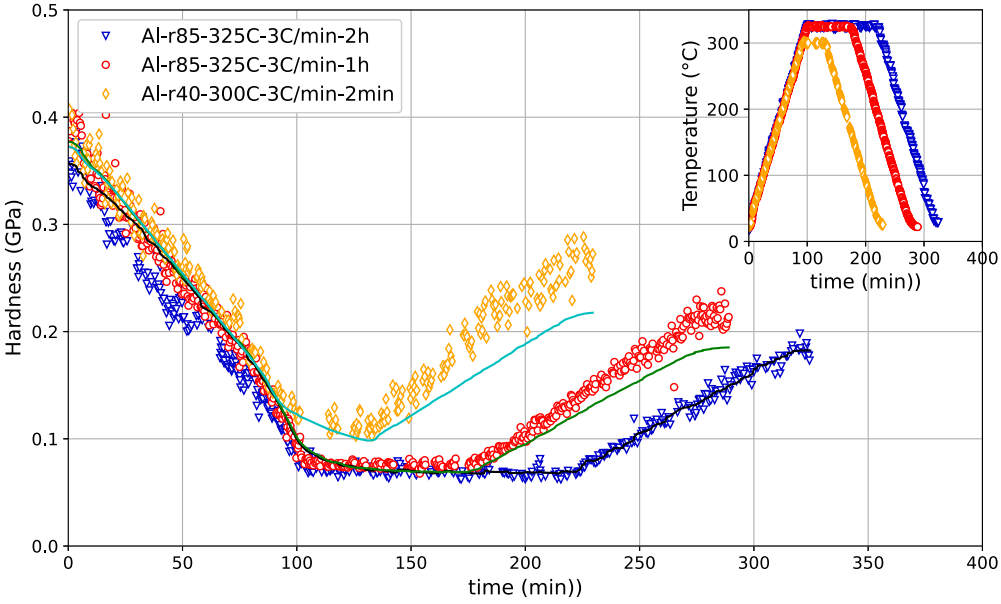

Fig. 11. Reconstruction of hardness changes for cold-rolled samples Al-r85-325C-3C/min-1h (green) and Al-r85-300C-3C/min-30min (cyan). Parameters were determined on sample Al-r85-325C-3C/min-2h (black). The model and the experimental data are in good agreement during the heating and the holding at maximum temperature.

covery and recrystallization are capable of successfully reconstructing the hardness variations observed in the samples used for their evaluation, as shown in Fig. 10.

6.2.4. *Predicting microstructure changes*

The reconstruction of hardness changes for samples Al-r85-325C-3C/min-1h and Al-r85-300C-3C/min-30min is shown in Fig. 11. Overall, the model demonstrates good consistency during the heating and holding segments, although a slight discrepancy is observed at the beginning of the hold segment. Additionally, the model underestimates the hardness increase during cooling. These discrepancies suggest that there might be room for improvement in the fitting of the recrystallization process.

It is worth noting that the model relies on certain assumptions regarding the variation of the activation of plastic flow. Specifically, it assumes that the parameter a_0 is independent of the thickness reduction ratio and does not vary significantly with temperature. Furthermore, the assumption of a mixture law between a_0 and a_{ReX} in temperature, as used in equation S18, may not accurately capture the true behavior of the activation plasticity parameter. Further refinements in the modeling approach and additional experimental data could help improve the accuracy of the recrystallization fitting and enhance the overall predictive capability of the model.

7. Discussion

In this paper, it is shown that a few well-chosen HTSI tests can discriminate thermally activated restoration mechanisms in cold-rolled pure aluminum and copper samples. This ability is a direct result of the HTSI method, which combines rapid loading cycles and high-temperature nanoindentation methods, resulting in a significant number of data points throughout the thermal path [20,21]. This represents a clear advantage over conventional high-temperature nanoindentation testing [19,18,48], which requires a slow regulation procedure to limit thermal drift during mechanical loading and typically yields only a few nanohardness measurements per day of testing.

The dataset obtained through HTSI testing is somewhat comparable to that obtained from Dynamic Scanning Calorimetry measurements [11,12], albeit based on the sensing of mechanical properties. It offers similar advantages, particularly the ability to detect material transformations occurring during specific thermal paths, provided that these transformations significantly affect mechanical properties. For example, the HTSI method shows promise for screening the recrystallization temperature of a particular alloy class based on its composition for a given thermal path. This applicability can be extended to other metallurgical phenomena such as precipitation hardening or phase transformation.

As demonstrated in the study conducted on cold-rolled aluminum, the HTSI method enables the discrimination of various metallurgical mechanisms within the same temperature range by manipulating thermal paths and initial sample states. The next phase involves using the HTSI method to quantify transformation kinetics, which necessitates the application of metallurgical models with a set of parameters to be identified. This paper proposes the use of standard models [5,6,23,25–27] developed for recrystallization and recovery in conjunction with an inverse identification method. The success of this approach is primarily reliant on the quality of the experimental data.

The models employed in this study accurately reconstruct the hardness variations with time and temperature, exhibiting excellent agreement with HTSI experimental data. However, the significance of such quantification is compromised if the uniqueness and stability of the solutions cannot be ensured. To address this concern, the identifiability index proposed by Richard et al. [42,43] holds promise. In this paper, it is noted that the dataset is sufficiently comprehensive to quantify the kinetics of static recovery in cold-rolled aluminum, but precise quantification of recrystallization kinetics in both cold-rolled copper and cold-rolled aluminum proves challenging. Particularly, quantifying the incubation process from the available dataset is not straightforward.

This difficulty in quantification can be attributed to the nature of the incubation stage, which governs the initiation of the recrystallization process. As a stochastic process, it competes with recovery mechanisms. Increasing the number of HTSI tests would undoubtedly enhance the understanding of this process. Surprisingly, the quantification of subsequent recrystallization mechanisms, such as nucleation and growth, also faces challenges despite the excellent agreement observed in terms of hardness variations with time and temperature. The solutions obtained for both copper and aluminum are not unique and stable, which is an outcome of the inverse procedure attempting to quantify all parameters of various mechanisms within the same optimization step [42]. However, if the incubation stage were accurately quantified prior to the optimization procedure, the identifiability index would be lower.

Therefore, expanding the dataset through additional thermal paths is necessary.

In this paper, the quantification of microstructure modifications was solely based on hardness changes. However, it is important to note that the hardness measurements at a given temperature exhibit some standard deviation. This variability can be attributed to a combination of factors such as the size of the hardness imprints and the heterogeneity of the microstructure [49,50]. One interesting observation is that the standard deviation of hardness is higher during heating compared to cooling. This can be explained by the progressive transformation of the heterogeneous cold-rolled microstructure into a more homogeneous recrystallized microstructure during the thermal process.

Analyzing the variations in standard deviation with temperature can provide valuable insights for modeling microstructure changes. In this regard, statistical nanoindentation testing can be a useful tool [9]. By considering the statistical distribution of hardness measurements, it becomes possible to gain a more comprehensive understanding of the microstructural heterogeneity and its evolution during thermal treatments. Such information can contribute to the refinement and improvement of microstructure models.

Indeed, nanoindentation is a localized testing technique that provides information about the material's response in the first nanometers to micrometers beneath the surface. By conducting tests at different maximum depths during temperature experiments, it is possible to investigate variations in restoration kinetics due to the probed volume. This approach enables the study of phenomena at very local scales, providing valuable insights into the material's behavior.

To achieve this, it is necessary to implement an indentation cycle that performs tests at a specific maximum depth, rather than a maximum load, while varying the temperature. This allows for the examination of depth-dependent changes in mechanical properties and restoration mechanisms. By analyzing the material's response at different depths, differences in the kinetics of static recrystallization can be elucidated, providing a more comprehensive understanding of the phenomenon.

It is important to note that static recrystallization is inherently heterogeneous, and conducting tests at a very local scale may miss the initial moments of nucleation and growth. To overcome this limitation, a combination of spatial analysis techniques, specifically designed HTSI tests (such as those incorporating changing heating rates), and electron backscatter diffraction (EBSD) characterizations can be employed. This integrated approach would provide more comprehensive results and a deeper understanding of the observed behaviors, allowing for the exploration of microstructural evolution and the impact of local-scale variations on restoration mechanisms.

8. Conclusions

The High-Temperature Scanning Indentation method [20] has revolutionized the study of microstructural changes during thermal cycling by enabling the quasi-continuous measurement of mechanical properties. In this article, the restoration kinetics of cold-rolled pure aluminum and pure copper are investigated using the HTSI technique. It has been observed that the variations in hardness can be directly linked to microstructural modifications, indicating the occurrence of restoration mechanisms within the deformed structure. The objective of this paper is to quantify the kinetics of these processes.

The key points covered in this article are as follows:

- The HTSI method enables the study of microstructural changes in cold-rolled pure aluminum and pure copper samples during thermal ramping.
- Variations in hardness with temperature serve as clear signatures of the thermal activation of plastic flow, static recovery, and recrystallization processes.
- By combining basic models for static recovery and recrystallization, accurate quantification of restoration kinetics can be achieved.
- Static recovery is found to play a major role in the recrystallization kinetics of aluminum.
- No recovery is reported in pure copper, as expected due to its lower stacking fault energy.
- The effect of heating rates on recrystallization kinetics is observed to be opposite, depending on the presence or absence of static recovery.

This paper highlights that the HTSI method is a valuable tool for materials design. With a limited number of well-designed HTSI experiments, restoration kinetics can be quantified, allowing for the establishment of a relationship with alloy composition. Furthermore, the HTSI technique shows promise for investigating other metallurgical phenomena such as precipitation, phase transformation, and oxidation.

Funding

The authors acknowledge support from the CPER MANUTECH which financed the experimental system. This work was supported by the French National Research Agency (ANR) under contract ANR-20-CE08-0022.

Declaration of competing interest

The authors declare that they have no known competing financial interests or personal relationships that could have appeared to influence the work reported in this paper.

Data availability

The raw/processed data required to reproduce these findings cannot be shared at this time due to legal reasons.

Acknowledgements

The authors would like to thank Gilles Blanc for his assistance in preparing the samples for obtaining the fine EBSD measurements, Marilyne Mondon for her valuable time in conducting the EBSD experiments, and ChatGPT 3.5 for its assistance in language correction.

Appendix A. Supplementary material

Supplementary material related to this article can be found online at https://doi.org/10.1016/j.matdes.2023.112171.

References

[1] P.T. Summers, Microstructure-Based Constitutive Models for Residual Mechanical Behavior of Aluminum Alloys after Fire Exposure, Ph.D. thesis, 2014, Harvard.
[2] A. Durif, M. Richou, G. Kermouche, M. Lenci, J.-M. Bergheau, Impact of tungsten recrystallization on ITER-like components for lifetime estimation, Fusion Eng. Des. 138 (2019) 247–253.
[3] A. Durif, Modélisation de la durée de vie de composants face au plasma dans les réacteurs à fusion thermonucléaire, Ph.D. thesis, Université de Lyon, 2019.
[4] F.J. Humphreys, M. Hatherly, Recrystallization and Related Annealing Phenomena, Elsevier, 2004.
[5] E. Nes, Recovery revisited, Acta Metall. Mater. 43 (1995) 2189–2207.
[6] M. Verdier, Y. Brechet, P. Guyot, Recovery of AlMg alloys: flow stress and strain-hardening properties, Acta Mater. 47 (1998) 127–134.
[7] M.A. Vicente Alvarez, M. Marchena, T. Perez, Recovery kinetics of cold-deformed Cr-Mo steels, Metall. Mater. Trans. A 39 (2008) 3283–3290.
[8] R.A. Vandermeer, N. Hansen, Recovery kinetics of nanostructured aluminum: model and experiment, Acta Mater. 56 (2008) 5719–5727.
[9] L. Karanja, M. Lenci, D. Piot, C. Maurice, A. Durif, M. Richou, L. Gallais, M. Minissale, G. Kermouche, An attempt to assess recovery/recrystallization kinetics in tungsten at high temperature using statistical nanoindentation analysis, Crystals 11 (2020) 37.

[10] M. Richou, A. Durif, M. Lenci, M. Mondon, M. Minissale, L. Gallais, G. Kermouche, G. De Temmerman, Recrystallization at high temperature of two tungsten materials complying with the ITER specifications, J. Nucl. Mater. 542 (2020) 152418.
[11] M.J. Starink, A.-M. Zahra, An analysis method for nucleation and growth controlled reactions at constant heating rate, Thermochim. Acta 292 (1997) 159–168.
[12] J. Farjas, P. Roura, Modification of the Kolmogorov–Johnson–Mehl–Avrami rate equation for non-isothermal experiments and its analytical solution, Acta Mater. 54 (2006) 5573–5579.
[13] E.M. Lauridsen, H.F. Poulsen, S.F. Nielsen, D. Juul Jensen, Recrystallization kinetics of individual bulk grains in 90% cold-rolled aluminium, Acta Mater. 51 (2003) 4423–4435.
[14] A. Lens, C. Maurice, J.H. Driver, Grain boundary mobilities during recrystallization of Al–Mn alloys as measured by in situ annealing experiments, Mater. Sci. Eng. A 403 (2005) 144–153.
[15] E.M. Lauridsen, S. Schmidt, S.F. Nielsen, L. Margulies, H.F. Poulsen, D.J. Jensen, Non-destructive characterization of recrystallization kinetics using three-dimensional X-ray diffraction microscopy, Scr. Mater. 55 (2006) 51–56.
[16] N. Bozzolo, S. Jacomet, R.E. Logé, Fast in-situ annealing stage coupled with EBSD: a suitable tool to observe quick recrystallization mechanisms, Mater. Charact. 70 (2012) 28–32.
[17] F. Christien, M.T.F. Telling, K.S. Knight, R. Le Gall, A method for the monitoring of metal recrystallization based on the in-situ measurement of the elastic energy release using neutron diffraction, Rev. Sci. Instrum. 86 (2015) 053901.
[18] P. Baral, M. Laurent-Brocq, G. Guillonneau, J.-M. Bergheau, J.-L. Loubet, G. Kermouche, In situ characterization of AA1050 recrystallization kinetics using high temperature nanoindentation testing, Mater. Des. 152 (2018) 22–29.
[19] C. Minnert, W.C. Oliver, K. Durst, New ultra-high temperature nanoindentation system for operating at up to 1100 °C, Mater. Des. 192 (2020) 108727.
[20] G. Tiphéne, P. Baral, S. Comby-Dassonneville, G. Guillonneau, G. Kermouche, J.-M. Bergheau, W.C. Oliver, J.-L. Loubet, High-temperature scanning indentation: a new method to investigate in situ metallurgical evolution along temperature ramps, J. Mater. Res. 36 (2021) 2383–2396.
[21] S. Comby-Dassonneville, G. Tiphéne, A. Borroto, G. Guillonneau, L. Roiban, G. Kermouche, J.-F. Pierson, J.-L. Loubet, P. Steyer, Real-time high-temperature scanning indentation: probing physical changes in thin-film metallic glasses, Appl. Mater. Today 24 (2021) 101126.
[22] G. Saada, Sur le durcissement dû à la recombinaison des dislocations, Acta Metall. 8 (1960) 841–847.
[23] D. Kuhlmann, G. Masing, J. Raffelsieper, Zur Theorie der Erholung, Int. J. Mater. Res. 40 (1949) 241–246.
[24] J. Friedel, Dislocations, vol. 3, Pergamon Press, 1964.
[25] W.A. Johnson, R.F. Mehl, Reaction kinetics in processes of nucleation and growth, Trans. Am. Inst. Min. Metall. Eng. 135 (1939) 416–442.
[26] A. Kolmogoroff, Zur Statistik der Kristallisationsvorgange in Metallen, Izv. Akad. Nauk SSSR, Ser. Mat. 1 (1937) 355–359.
[27] M. Avrami, Kinetics of phase change. I General theory, J. Chem. Phys. 7 (1939) 1103–1112.
[28] W. Pantleon, Thermal stability of the microstructure in rolled tungsten for fusion reactors, Phys. Scr. 96 (2021) 124036.
[29] J.-L. Loubet, M. Bauer, A. Tonck, S. Bec, B. Gauthier-Manuel, Nanoindentation with a surface force apparatus, in: M. Nastasi, D.M. Parkin, H. Gleiter (Eds.), Mechanical Properties and Deformation Behavior of Materials Having Ultra-Fine Microstructures, Springer, Netherlands, Dordrecht, 1993, pp. 429–447.
[30] W.C. Oliver, G.M. Pharr, Measurement of hardness and elastic modulus by instrumented indentation: advances in understanding and refinements to methodology, J. Mater. Res. 19 (2004) 18.
[31] P. Sudharshan Phani, W.C. Oliver, A critical assessment of the effect of indentation spacing on the measurement of hardness and modulus using instrumented indentation testing, Mater. Des. 164 (2019) 107563.
[32] F. Bachmann, R. Hielscher, H. Schaeben, Grain detection from 2d and 3d EBSD data—specification of the MTEX algorithm, Ultramicroscopy 111 (2011) 1720–1733.
[33] F.J. Humphreys, Review grain and subgrain characterisation by electron backscatter diffraction, J. Mater. Sci. 36 (2001) 3833–3854.
[34] S. Primig, H. Leitner, W. Knabl, A. Lorich, H. Clemens, R. Stickler, Influence of the heating rate on the recrystallization behavior of molybdenum, Mater. Sci. Eng. A 535 (2012) 316–324.
[35] G. Kermouche, J. Loubet, J. Bergheau, Extraction of stress–strain curves of elastic–viscoplastic solids using conical/pyramidal indentation testing with application to polymers, Mech. Mater. 40 (2008) 271–283.
[36] J. Go, W.J. Poole, M. Militzer, M.A. Wells, Modelling recovery and recrystallisation during annealing of AA 5754 aluminium alloy, Mater. Sci. Technol. 19 (2003) 1361–1368.
[37] D. Caillard, J.-L. Martin, Thermally Activated Mechanisms in Crystal Plasticity, Pergamon Materials Series, vol. 8, Pergamon, Amsterdam, Boston, Mass, 2003.
[38] J. Kennedy, R. Eberhart, Particle Swarm Optimization, Proceedings of ICNN'95 - International Conference on Neural Networks, vol. 4, IEEE, Perth, WA, Australia, 1995, pp. 1942–1948.
[39] R. Eberhart, J. Kennedy, A new optimizer using particle swarm theory, in: MHS'95, in: Proceedings of the Sixth International Symposium on Micro Machine and Human Science, IEEE, Nagoya, Japan, 1995, pp. 39–43.
[40] P.J. Angeline, Using selection to improve particle swarm optimization, in: 1998 IEEE International Conference on Evolutionary Computation Proceedings. IEEE World Congress on Computational Intelligence (Cat. No. 98TH8360), IEEE, Anchorage, AK, USA, 1998, pp. 84–89.
[41] Y. Shi, R. Eberhart, A modified particle swarm optimizer, in: 1998 IEEE International Conference on Evolutionary Computation Proceedings. IEEE World Congress on Computational Intelligence (Cat. No. 98TH8360), IEEE, Anchorage, AK, USA, 1998, pp. 69–73.
[42] F. Richard, M. Villars, S. Thibaud, Viscoelastic modeling and quantitative experimental characterization of normal and osteoarthritic human articular cartilage using indentation, J. Mech. Behav. Biomed. Mater. 24 (2013) 41–52.
[43] S. Breumier, S. Sao-Joao, A. Villani, M. Lévesque, G. Kermouche, High strain rate micro-compression for crystal plasticity constitutive law parameters identification, Mater. Des. 193 (2020) 108789.
[44] A.M. Wusatowska-Sarnek, H. Miura, T. Sakai, Influence of deformation temperature on microstructure evolution and static recrystallization of polycrystalline copper, Mater. Trans. 42 (2001) 2452–2459.
[45] E.A. Jägle, E.J. Mittemeijer, The kinetics of and the microstructure induced by the recrystallization of copper, Metall. Mater. Trans. A 43 (2012) 1117–1131.
[46] M. Seyed Salehi, N. Anjabin, Modeling and experimental study of static recovery and mechanical behavior of AA5052 alloy during cold-working and subsequent annealing, Iran. J. Mater. Forming 4 (2017) 28–38.
[47] J.M. Wheeler, V. Maier, K. Durst, M. Göken, J. Michler, Activation parameters for deformation of ultrafine-grained aluminium as determined by indentation strain rate jumps at elevated temperature, Mater. Sci. Eng. A 585 (2013) 108–113.
[48] J. Kappacher, M. Tkadletz, H. Clemens, V. Maier-Kiener, High temperature nanoindentation as a tool to investigate plasticity upon phase transformations demonstrated on cobalt, Materialia 16 (2021) 101084.
[49] V. Herrmann, K. Unseld, H.-B. Fuchs, The scale behavior of fillers in elastomers by means of indentation tests, Colloid Polym. Sci. 280 (2002) 267–273.
[50] P. Baral, C. Fradet, F. Lacroix, E. Le Bourhis, G. Guillonneau, G. Kermouche, J.-M. Bergheau, J.-L. Loubet, Extrinsic measurement of carbon black aggregate distribution within a fluoroelastomer matrix from nanoindentation experiments, ACS Appl. Mater. Interfaces 12 (2020) 6716–6726.